Zhou *et al.*
EURASIP Journal on Advances in Signal Processing (2024) 2024:88
https://doi.org/10.1186/s13634-024-01185-5

EURASIP Journal on Advances in Signal Processing

RESEARCH Open Access

Identifying sources of interference in civil aviation radio communication

Mingsheng Zhou[1], Mingming Kong[1*], Yuan Ye[2], Binbin Deng[1] and Yulin Tang[3]

*Correspondence:
kongming000@126.com

[1] School of Computer and Software Engineering, Xihua University, ChengDu 610039, SiChuan, China
[2] Ningxia Hui Autonomous Region Radio Management Committee Office, YinChuan 750000, NingXia, China
[3] Sichuan Radio Monitoring Station, ChengDu 610052, SiChuan, China

Abstract

Civil aviation is an important part of public transportation. However, the wireless communication systems used in the approach and tower control phases of traffic control are susceptible to external interference, posing a threat to flight safety. Traditional communication interference solutions are time-consuming and require specialized technicians to troubleshoot. To solve this problem, we propose a real-time method for monitoring abnormal signals and detecting interference sources during aviation radio communications. The method consists of three steps: real-time blind source signal separation using cubic polynomial fitting, abnormal signal monitoring based on discriminative signal residence time, and using Pearson correlation coefficients to identify abnormal interference sources. This comprehensive approach effectively ensures the frequency safety of aviation radio communications. Experiments conducted at different locations in real airport environments demonstrate that this method can efficiently identify the signal bands and their interference sources.

Keywords: Air traffic control, Air traffic security, Avionics security, Radio interference identification

1 Introduction

The rapid development of radio and related technologies in aviation communications has greatly improved air transportation safety, but many challenges remain. According to the International Civil Aviation Organization (ICAO), civil aircraft go through five scheduling stages during air traffic control procedures: tower control, approach control, area control, approach control, and tower control. During the tower control and approach control stages, the safe use of non-directional beacons, very high frequency (VHF) omnidirectional beacons, rangefinders, and instrument landing systems is crucial for civil aviation flight safety, directly affecting passenger safety. The frequency security of VHF omnidirectional beacons is particularly threatened by radio interference from the adjacent frequency modulation (FM) broadcast band [1, 2]. Radio interference refers to unwanted energy from emissions, radiation, induction, or a combination that affects radio communication system reception, reducing performance or making the signal unreceivable. Most interference is caused by illegal broadcasting, irregular installation of radio transmission antennas, and radio transmitting stations not meeting standards,

leading to interference with the civil aviation communication band [3, 4]. Interfering signals pose a challenge to radio regulation [5–7].

In the event of radio interference during civil aviation flights, the traditional method involves the civil aviation department submitting a complaint to the radio management department. This is followed by the opinions of the monitoring station, frequency and station section, and law enforcement inspection section. Finally, the relevant radio monitoring station organizes technical forces to resolve the issue. This process typically includes large-scale road tests, air exclusion [8], and other methods. However, the lack of information on flight status and the electromagnetic environment often results in high costs and prolonged troubleshooting, which may cause optimal monitoring opportunities to be missed. Scholars have proposed solutions such as antenna isolation, optimizing filters, attaching anti-jamming devices [9], and implementing policy measures [10] to address these issues.

We propose a novel method for monitoring abnormal signals and identifying interference sources in aviation radio communication using real-time digital sweep spectrum. First, we extract signals from the monitored frequency band, then determine abnormal signals in the aviation frequency band, and finally identify interference source signals. Experiments conducted at several monitoring locations in a specific airfield confirmed the feasibility of the proposed method. The main contributions of this study are as follows:

- *Adaptive signal extraction:* We utilize cubic polynomial fitting to determine the discriminant between signal and noise in real time, which is then used to determine an adaptive threshold line for separating the signals from the noise.
- *Abnormal signal identification:* Within the civil aviation communication band, we identify abnormal signal bands by evaluating the signal residence time after adaptive signal extraction.
- *Interference source identification:* We use the Pearson correlation coefficient to evaluate the correlation between the abnormal signal and other signals to determine the interference source of the abnormal signal.

2 Spectrum management and abnormal detection

With the rise of smart terminals and the launch of various ultra-broadband services, radio spectrum resource management faces serious challenges like scarce spectrum resources, low utilization rates, and the abuse of illegal stations. Recent research aims to accurately describe the utilization of spectrum resources using the spectrum map. This technique projects the received signal strength onto the geographic coordinates of the area of interest, providing a clear picture of the signal strength distribution in space. Currently, spectrum map construction schemes are categorized into two main classes: spatial correlation-based and joint frequency-space correlation-based. The former uses the spatial correlation of spectral signals, while the latter considers both joint frequency and spatial correlation to assess spectral signal strength for constructing the spectrum map [11–13]. Monitoring utilization can effectively address the problem of spectrum resource allocation and utilization [14–16]. However, this does not completely solve the problem of interference from illegal stations to normal station signals in radio spectrum

resource management. This issue is particularly prominent in civil aviation communications, where the security of radio communications between towers and pilots is crucial.

In the tower control and approach control phases of civil aviation, the Air Traffic Controller (ATC) uses the civil aviation communication band (108MHz~137MHz) to communicate with pilots. During our radio monitoring near several airports, we found more illegal broadcasts in the adjacent FM radio band (87MHz~108MHz). These illegal broadcasting devices do not meet the relevant transceiver entry specifications, and the signals they emit may cause issues like intermodulation and spurious signals. These issues can propagate into the civil aviation communication band, interfering with the normal operation of air traffic control [3, 4]. Current solutions mainly rely on manual listening by professional technicians to track abnormal signals. However, this approach faces challenges such as difficulty in manual monitoring, delayed response, and high operational costs. To address the problem of monitoring abnormal signals and illegal stations in the civil aviation communication band, we propose a signal correlation-based method for monitoring abnormal signals and identifying interference sources. The method consists of three key steps: signal extraction for the FM radio band and the civil aviation communication band (refer to Sect. 3), monitoring abnormal signals in the civil aviation communication band (refer to Sect. 4), and identifying the sources of interference signals (refer to Sect. 5). Through this approach, we aim to improve monitoring efficiency and reduce dependence on manual listening, enabling timely and accurate detection and response to abnormal signals and illegal stations in the civil aviation communications frequency band.

3 Signal extraction

In the digital panoramic scanning spectrum of the dedicated civil aviation radio band and its neighboring FM broadcasting band, the signal band has a stable higher waveform, while the noise has a random lower waveform [17–20]. To enable real-time monitoring and early warning of abnormal spectrum activity in the aviation communication band, blind source signal extraction is essential. We propose an algorithm based on cubic polynomial fitting to obtain an adaptive threshold line that separates the signal and noise waveforms of the current spectrum frame and performs signal-to-noise separation for subsequent spectrum frames. This approach aids in identifying interference sources.

Specifically, signal extraction involves four steps: **1)** Perform data preprocessing on the digitally scanned spectral data to obtain the Mean Spectrum (MS) frames. **2)** Obtain two feature vectors of the mean spectra. **3)** Compute a cubic polynomial fitting on the feature vectors to derive the discriminant value. **4)** Use the discriminant value to obtain the signal-to-noise separation threshold line and extract the signal of the monitoring band.

3.1 Data preprocessing

We continuously acquire radio digital panoramic signal data by uninterrupted panoramic scanning (PSCAN) of the FM broadcast band (87MHz~108MHz) and the aviation communication band (108MHz~137MHz) with a radio digital receiver. A frame of radio digital panoramic scanning signal data is, at time t, a sequence of level values for all frequency points, the frequency points are denoted as $f^t = \{f_1^t, f_2^t, ..., f_m^t\}$, where m represents the number of frequency points. At a certain moment, the sequence composed of

the level values of each frequency point can be expressed as $sig = \{l_{f_1^t}, l_{f_2^t}, ..., l_{f_i^t}, ..., l_{f_m^t}\}$, where $l_{f_i^t}$ denotes the level value of the signal at the i-th frequency point. All the spectral signal frames in the time domain are acquired without interruption, and the consecutive n frames of spectral data are represented as $M_n = \{sig_1, sig_2, ..., sig_i, ..., sig_n\}$. sig_i represents a moment of panoramic scanning data. Our collected data comes from the R&S EM100 radio digital receiver.

Due to the influence of the complex electromagnetic environment on the monitoring band, i.e., the 'burr phenomenon' of the spectrum, it is necessary to pre-process the spectrum data. Whenever n consecutive frames of spectrum data are acquired, as Fig. 1, time-domain smoothing is performed to obtain a frame of Time-domain Mean Spectrum (TMS), i.e., the mean of the n level values of each frequency point is taken as the value of the corresponding frequency point in TMS. Then, a one-dimensional smooth convolution is performed on the TMS, where the convolution kernel is $[\frac{1}{4}, \frac{2}{4}, \frac{1}{4}]$, to obtain a frame of Mean Spectrum (MS) [21]. The spectrum data acquisition window size n is related to the performance of the signal acquisition equipment. For the R &S EM100 digital receiver, we set $n = 10$. When the window size is small, the mean spectrum struggles to filter out spectral perturbations caused by environmental abnormalities. Conversely, when the window size is large, it becomes challenging to accurately characterize short-time local signal features.

3.2 Obtaining feature vectors

The radio digital swept spectrum consists of a signal waveform and a noise waveform, each with a left rising edge and a right falling edge. The waveform height reflects the intensity of the spectrum data level values. By analyzing the characteristics of the radio digital sweep spectrum data, we know that the signal waveform presents a stable, higher waveform, while the noise shows a lower waveform with irregular changes. There is a discriminating value between their waveform heights, with heights lower than this value being noise waveforms. Finding this discriminant value effectively separates the signal from the noise in the spectral data frame. To better characterize the spectral data frames, we first obtain the heights of the left and right edges of all waveforms based on the level values of the digitally swept

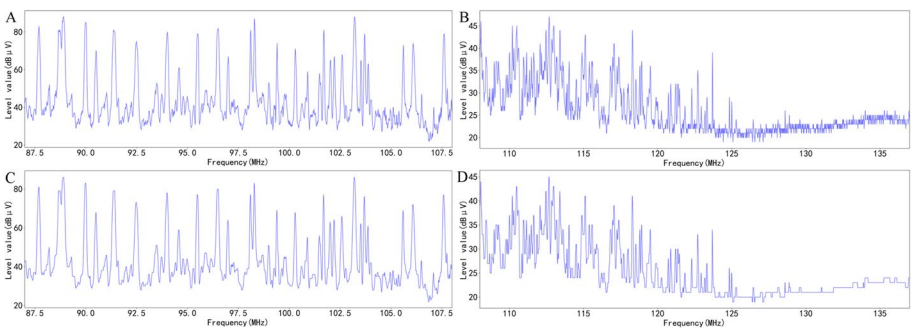

Fig. 1 Smooth process. The figure shows the TMS and MS computed from n consecutive randomly selected frames on the 87MHz~137MHz frequency band.[**A, B**] is the TMS obtained after time-domain smoothing, and [**C, D**] is the MS obtained by convolutional smoothing of the TMS

spectra. These are then quantized into two feature vectors. These two sets of feature vectors are used to find the discriminating values between signal and noise waveforms.

In MS, peaks and troughs are defined as follows: the frequency point in the middle of a local maximum or multiple maximums is a peak, and the frequency point in the middle of a local minimum or multiple minimums is a trough. The level value of the adjacent peak is greater than the level value of the trough.

The left rising edge height (h^L) and right falling edge height (h^R) are defined as follows: the difference between a peak and its adjacent left trough forms the left rising edge height array (H_L). The difference between a peak and its adjacent right trough forms the right falling edge height array (H_R). H_L and H_R are one-dimensional arrays with all positive values. These two vectors are the digital sweep feature vectors of the current MS frame.

3.3 Calculate the discriminating value

Since the left rising edge and right falling edge in the spectrum waveform may be affected by nearby waveforms, we need to calculate the discriminant values for the left and right using H_L and H_R, respectively. To adaptively obtain the difference between the signal and noise waveforms, we perform a cubic polynomial fitting [22] on the two arrays after sorting them in ascending order ($h_L^{'}$ and $h_R^{'}$). This gives us a discriminant value for judging the difference between the signal and noise waveforms. Specifically, as Fig. 2, for the sorted left rising edge array, there is a noticeable change in intensity between the waveform with smaller energy and the waveform with larger energy. We fit the $h_L^{'}$ to obtain $F_L = a \times x^3 + b \times x^2 + c \times x + d$. If $\Delta > 0$, where $\Delta = b^2 - 3 \times a \times c$, the stationary point I_{min}^L of F_L is calculated, where

$$I_{min}^L = \lfloor \frac{\sqrt{\Delta} - b}{3 \times a} \rfloor \tag{1}$$

If $\Delta \leq 0$, I_{min}^L is the point in F_L with slope 0, find the height in $h_L^{'}$ that corresponds to L_{min} as the left discriminant, where

$$I_{min}^L = \lfloor \frac{-b}{3 \times a} \rfloor \tag{2}$$

As Fig. 2, $\Delta > 0$, I_{min}^L=81, the left discriminant value $h_{noise}^L = h_L^{'}(I_{min}^L) = 6$, and the same procedure may be easily adapted to obtain the right discriminant value

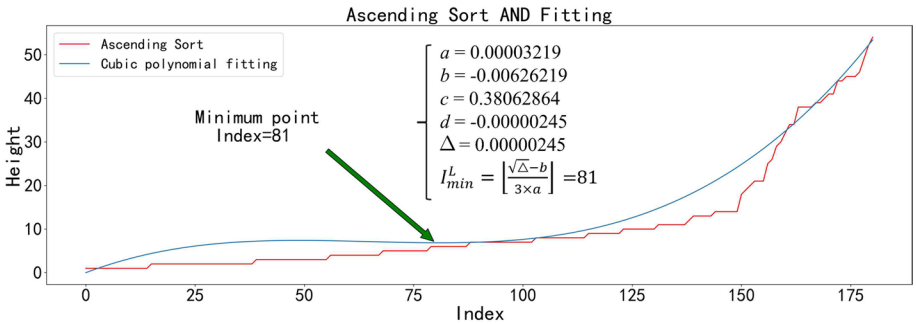

Fig. 2 Ascending sort and Fitting. The horizontal coordinate is the vector index. The vertical coordinate is the vector value, which corresponds to the difference (Height) of the level value directly between the crest and the trough

$h^R_{noise} = h'_R(I^R_{min}) = 6$, and the final discriminant value $h_{noise} = 6$ is obtained by taking the average value of the h^L_{noise} and h^R_{noise} by comprehensive consideration.

3.4 Obtaining the signal–noise separation threshold line

The calculated h_{noise} represents the intensity of the mutation level for all waveforms in the monitoring band. We obtain a frame of signal-to-noise separation threshold line by scaling the MS equally and use it to extract signals for the subsequent $n = 10$ consecutive frames of spectral data.

Our approach is that, for any waveform, the frequency points between its left trough and peak, and the frequency points between its right trough and peak, are scaled separately. Specifically, for any waveform in an MS, all frequency points are scaled equally based on the percentage of the level value of that frequency point in the corresponding left rising edge or right falling edge (including the peaks and excluding the troughs), based on the line connecting the two troughs in this waveform.

For the frequency points between the peak and the adjacent left trough of any waveform, the scale equation is

$$\begin{aligned} MS(f_{k_i}, L_{k_i}) &= S(L_{k_i}, h_{\text{noise}}) + O(k_i) \\ &= \left(\frac{L_{k_i} - L_{k_1}}{h^L}\right) \times h_{\text{noise}} \\ &\quad + \left[\left(\frac{L_{k_2} - L_{k_1}}{k_2 - k_1}\right) \times (k_i - k_1) + L_{k_1}\right] \end{aligned} \tag{3}$$

For the frequency points between the peak and the adjacent right trough of any waveform, the scale equation is

$$\begin{aligned} MS(f_{k_i}, R_{k_i}) &= S(R_{k_i}, h_{\text{noise}}) + O(k_i) \\ &= \left(\frac{R_{k_i} - L_{k_1}}{h^R}\right) \times h_{\text{noise}} \\ &\quad + \left[\left(\frac{L_{k_2} - L_{k_1}}{k_2 - k_1}\right) \times (k_i - k_1) + L_{k_1}\right] \end{aligned} \tag{4}$$

where, $S(L_{k_i}, h_{noise})$ and $S(R_{k_i}, h_{noise})$ are the scaling term, $O(k_i)$ is the offset term, L_{k_1} is the level value of the frequency point f_{k_1} at the left trough, L_{k_2} is the level value of the frequency point f_{k_2} at the right trough, f_{k_i} is a frequency point of that waveform, $k_i \in [k_1 + 1, ..., k_2 - 1]$, L_{k_i} and R_{k_i} are the level value of the frequency point f_{k_i} corresponding to the left rising edge or the right falling edge. The scaling term is used to obtain the relative level value of the threshold line by scaling h_{noise} equiproportionally for the intensity of the level value of the frequency point in the waveform in which it is located. The offset term corrects the scaled level value by using the line connecting the left and right troughs of the corresponding waveform as the baseline.

The signal–noise separation threshold line is obtained by scaling the MS using the discriminating value h_{noise}, which is calculated by evaluating the intensity of the mutation level of n consecutive frames of spectrum data. The scaling equations 3 and 4 substantially suppress the level values of the signal band, while the noise band level values are not suppressed. This allows the threshold line to perform signal extraction for the subsequent n frames of the spectrum. As Fig. 3, using an example of an electromagnetic

environment with many abnormal signals in the aviation communication band, the subsequent frames of the collected spectrum are compared with the threshold line. The band where the level value of the corresponding frequency point exceeds the threshold line is identified as a signal band.

4 Abnormal signal monitoring

During the tower control and approach control phases of the air traffic control process, the Air Traffic Controller (ATC) communicates with the pilot via radio using half-duplex communication. High-quality audio is essential to ensure the control process is carried out safely. However, abnormal FM broadcasts or air traffic signals can generate radio interference, leading to deterioration of signal reception, information errors or loss, or even blocking communication.

To distinguish abnormal signals from normal ones in the aviation communication band, we analyzed the operating characteristics of civil aviation communication services. In the professional field, standard terms are concise, easy to understand, and effective in avoiding ambiguity. They are the most direct and effective tool for communication between professionals. We continuously observed the communication signals between ATC and the pilot, combining this with the special call sign terminology assigned by the International Civil Aviation Organization (ICAO). We concluded that the dwell time of a single voice communication signal between ATC and the pilot via radio is usually less than 5 s. Therefore, we continuously monitor the spectrum data and signal extraction in the VHF band from 87MHz to 137MHz. When a signal is acquired, a Signal Dwell Time Listener (SL) is set at the location of the corresponding signal band, and the monitoring cycle of this SL will work until the signal disappears. The SL uses a multi-threaded

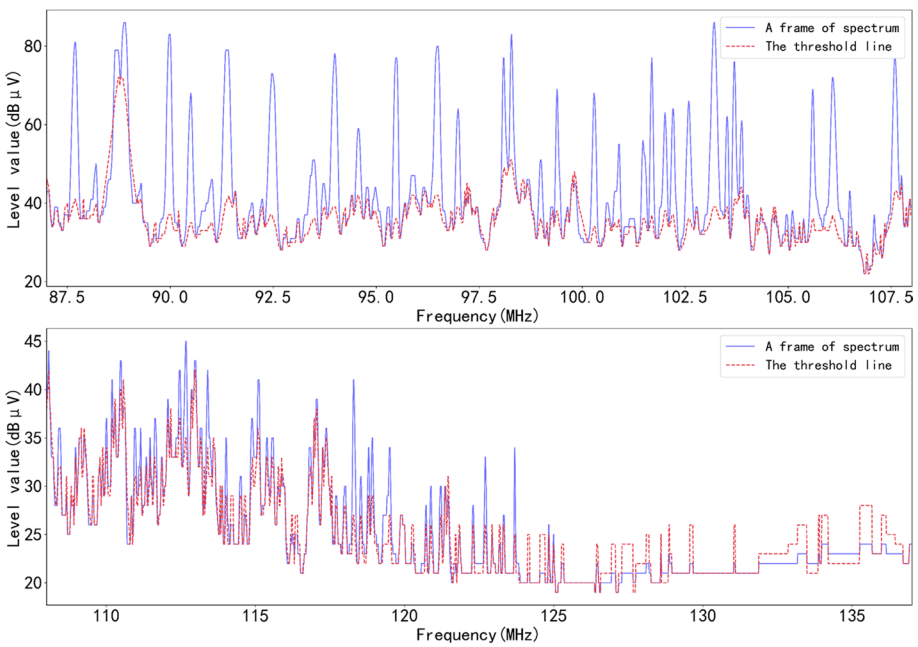

Fig. 3 Threshold line. A threshold line is obtained from the previous *n* frames of spectral data, and signal-to-noise separation is performed on the current *n* frames of spectral data. This image gives a visualization of the current frame in relation to the threshold line

concurrency technique. When the signal dwell time is less than 5 s, it is determined to be a normal communication signal; otherwise, it is an abnormal signal.

Since the signal dwell time listener depends on the result of the presence or absence of the signal obtained from the signal extraction step, errors in signal dwell time discrimination can occur due to the misidentification of a few spectral frames. While the number of misidentified or missed signals during periods of dense signal occurrence is small, it affects the overall residence time discrimination of the signals.

We employ morphological closure operations [23] on binary images to address errors caused by complex electromagnetic environments [24] during signal extraction. For binary images, the morphological closure operation is a method based on binary information in an image with pixel values of 0 or 1. This operation adjusts and changes the connection state of elements in a matrix through a combination of expansion and erosion operations. By alternately applying erosion and expansion, morphological closure operations can smooth objects in a binary image while preserving their overall shape. This process helps remove noise and connect neighboring regions.

As Fig. 4, 10 windows (100 frames of the spectrum) are used as Signal Dwell Time Listening Windows (SLW). A two-dimensional matrix storing binary data represents the result of signal–noise separation, where 0 indicates noise and 1 indicates a signal. A 3×3 convolutional kernel is used to perform the morphological closing operation [25] on SLW. This operation addresses signal recognition errors caused by the complex electromagnetic spectrum environment from a macroscopic perspective, making the judgment of signal residence time more accurate. The dwell time of each signal is then judged separately, and any signal band with a dwell time of more than 5 s is marked as an abnormal signal.

5 Interference source identification

Abnormal signals can be classified as those directly generated by a transmitter or those indirectly generated and falling into the aviation communication band, affecting normal communication. Based on abnormal signal monitoring, we further identify the frequency band of the interference source signal for indirectly generated

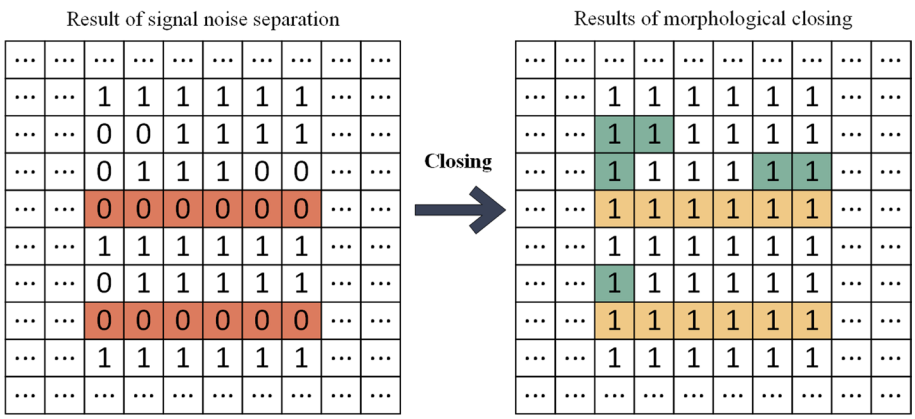

Fig. 4 Morphological closing. The red fill is the wrong signal extraction, the right matrix is the result after and the morphological closing operation repair

abnormal signals. Abnormal signals for which the source of interference cannot be found are considered to be directly generated.

The abnormal signal monitoring phase requires identifying all abnormal signal bands to provide information for subsequent interference source identification. Abnormal signals are unwanted energy generated by other signals that are emitted, radiated, induced, or intermodulated, degrading reception performance or preventing the reception of the target signal. Our goal is to identify the sources of interference for these abnormal signals.

As Fig. 5, the abnormal signal represents the portion of the interference source signal that leaks into other frequency bands. Typically, the level values of the interference source signal and the abnormal signal have a proportional relationship, and there is some degree of synchronization between the interference source and the corresponding frequency point of the interfered signal [26]. In other words, in a panoramic scanning spectral signal frame, the abnormal signal is not related to the intensity of

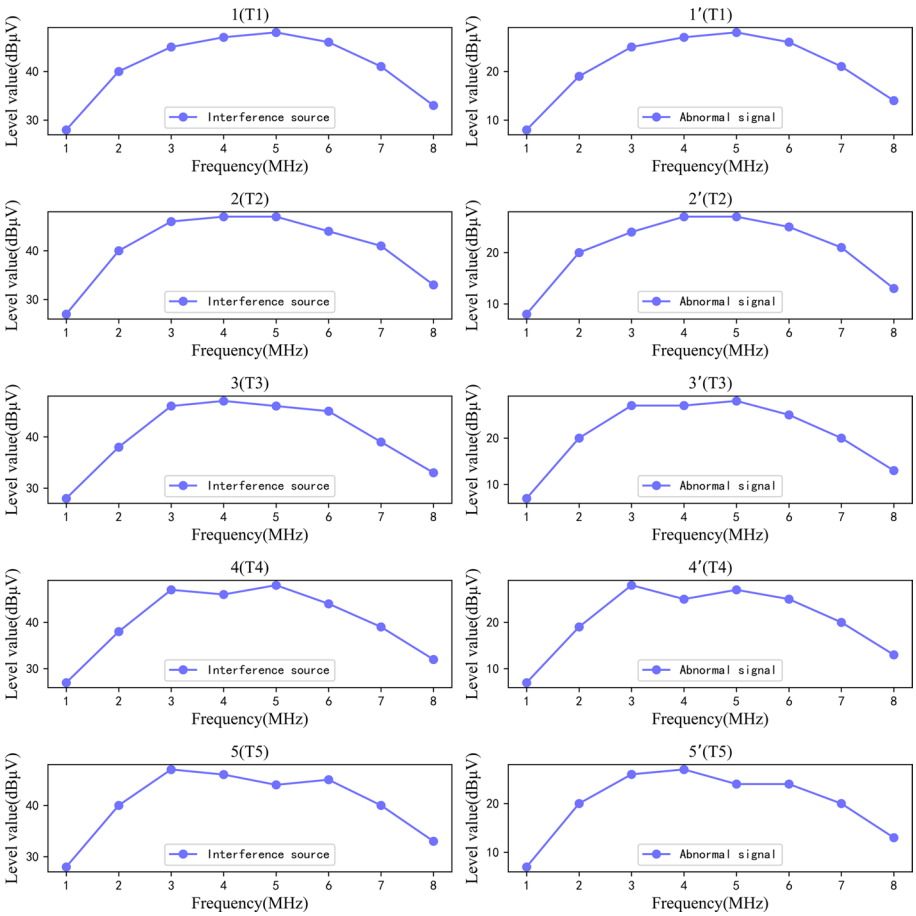

Fig. 5 Synergistic relationship. (1-5) is an interference source signal spectrum at the time of [T1-T5], ($1^{'}-5^{'}$) is an abnormal signal spectrum at the time of [T1-T5], and the level values of the abnormal signal and the interference source signal for the frequency points shows a trend of synchronous change. The correlation coefficients for the corresponding frequency points are [−0.17, 0.17, 0.57, 0.61, 0.78, 0.42, 0.91, 0.25], with an average correlation coefficient of 0.44. The two signals show a high degree of correlation

the interference source signal's level value but only to the degree of synchronization of the change in signal level values.

When an abnormal signal is detected, we search for its interference source in the monitoring band by assessing the correlation between the abnormal signal and other signals (excluding the abnormal signal itself). The signal with the highest correlation is identified as the interference source. To measure the correlation between two frequency points, we use the Pearson correlation coefficient [27]:

$$r = \frac{\sum_{i=1}^{n} \left(X_i - \bar{X}\right)\left(Y_i - \bar{Y}\right)}{\sqrt{\sum_{i=1}^{n} \left(X_i - \bar{X}\right)^2} \sqrt{\sum_{i=1}^{n} \left(Y_i - \bar{Y}\right)^2}} \tag{5}$$

For a monitoring window of consecutive n frames, $X = [X_1, ..., X_i, ..., X_n]$, $Y = [Y_1, ..., Y_i, ..., Y_n]$, X denotes the sequence of level values at one of the frequency points in the abnormal signal band. Y denotes the sequence of level values at the corresponding frequency point of any other signals. $\bar{X}$ is the mean value of X, and $\bar{Y}$ is the mean value of Y. For these two signal bands, the Pearson correlation coefficients are calculated separately for all the signal frequency points, and their average values are taken as the final correlation coefficients. As Fig. 5, the abnormal signals and the corresponding interference source signals we collected from the real environment, after calculating the correlation coefficients of the eight frequency points, respectively, the mean value is taken as the final correlation coefficient of 0.44, which means that the intensity change of their level values shows a strong positive correlation.

For both abnormal and other signals, when calculating the correlation degree between an abnormal signal and another signal, we use equally spaced mean downsampling to address the problem of different bandwidths. Since the abnormal signal is caused by partial energy leakage from the interfering source, its bandwidth is usually narrower than that of the interfering source signal. The Pearson correlation coefficient focuses on the trend of individual frequency points over time and is not affected by the change in amplitude. Therefore, equally spaced mean downsampling is performed on the wide bandwidth signal so that its bandwidth matches that of the narrow bandwidth signal. This retains the information about the change in leakage energy. Then, the correlation degree is calculated for all corresponding frequency points. Finally, the mean value of all correlation degrees is combined with the correlation degree of these two signals. The two signals with the highest correlation coefficients among the abnormal and other signals are identified as the interference sources.

6 Experiment

We performed several sets of experiments in different environments at various distances around a certain airport. We analyzed the effectiveness of signal extraction, abnormal signal monitoring, and interference source identification, verifying that the method is feasible.

As Fig. 6, we used the R&S EM100 digital receiver and HE600 antenna for data acquisition. For device connection, TCP and UDP connections were established between the PC and EM100. First, the PC sends Standard Commands for Programmable Instruments (SCPI) [28] to the EM100 via TCP, and then the EM100 returns

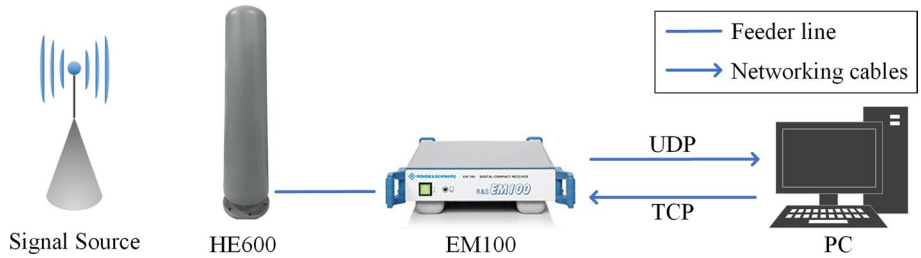

Fig. 6 Method of connecting radio receiving equipment

Table 1 Experimental data from different locations

Distance (km)	FM-SRR (%)	FM-SMR (%)	AM-SRR (%)	AM-SMR (%)	ASRR	ASMR	ISRR	ISCR
1	100	0	100	0	–	–	–	–
2	80	0	84	2	90%	0%	16.6%	66%
10	100	5	90	0	–	–	–	–
20	98.5	4	97	10	70%	0%	22.7%	80%

monitoring data to the PC via UDP. We acquired 87MHz~137MHz of digital panoramic scan data at a sampling step of 6.25 kHz. The data on which this article is based are available in [29].

6.1 Signal extraction experiment

Table 1 shows the Signal recognition rate (SRR) and Signal misrecognition rate (SMR).

$$\mathrm{SRR} = \frac{\mathrm{R}}{\mathrm{U}} \times 100\%, \mathrm{SMR} = \frac{\mathrm{M}}{\mathrm{U}} \times 100\% \tag{6}$$

where U is the number of signal bands identified as signals by the technician, R is the number of signal bands correctly identified by our algorithm, and M is the number that is misidentified. SRR$\in$ [0%, 100%], SMR$\in$ [0%, $+\infty$). SRR and SMR are distinguished by the prefixes 'FM-' and 'AM-' in the FM broadcast and aviation communication bands, respectively.

As Fig. 7, we collected spectrum data at 1 km (P1), 2 km (P2), 10 km (P3), and 20 km (P4) from a certain airport. P1 and P3 are west of the airport, while P2 and P4 are east of the airport. Both P1 and P3 are open spaces with a favorable environment, where no abnormal signals were discovered, and the recognition effect is good. The P4 experimental location, in the approach phase, is on the roof of a tall building. Here, the data acquisition effect is good and there are more abnormal signals, but the signal recognition rate is over 97%. Since the frequency occupancy of the aviation communication band varies between daytime and nighttime, we obtained relatively stable experimental data by conducting several experiments at different times of the day. Overall, our proposed blind source signal extraction method, based on cubic polynomial fitting, effectively identifies the interference sources of abnormal signals.

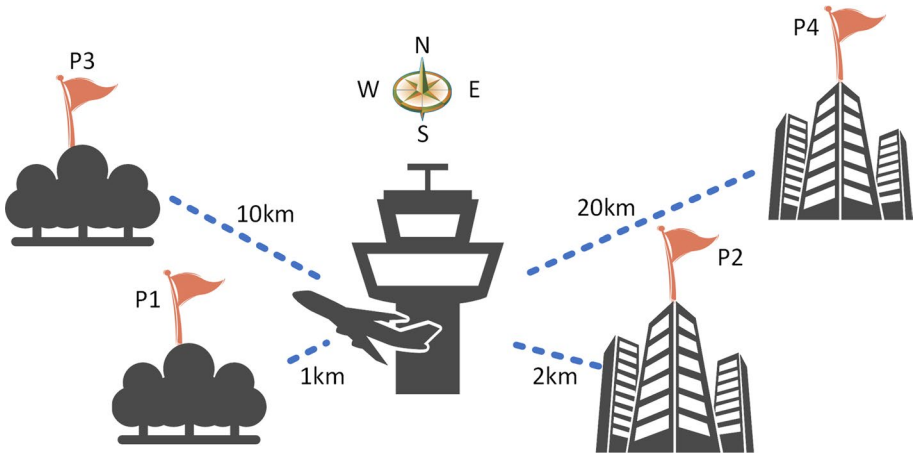

Fig. 7 Location of data acquisition

6.2 Interference source identification experiment

The accuracy of interference source identification will be affected by the accuracy of signal extraction and abnormal signal monitoring. But signal extraction experiments have confirmed the feasibility of following operations, so we analyze the rate of abnormal signal recognition and the accuracy of interference source identification by combining waterfall plots of digital panoramic scanning frequency spectrum and voice listening results.

As in Table 1, the abnormal signal recognition rate (ASRR), Abnormal signal misrecognition rate (ASMR), Interference source signal recognition rate (ISRR), and Interference source signal correct rate (ISCR) are obtained from different experimental locations.

$$\mathrm{ASRR} = \frac{\mathrm{AR}}{\mathrm{AU}} \times 100\%, \mathrm{ASMR} = \frac{\mathrm{AM}}{\mathrm{AU}} \times 100\% \tag{7}$$

$$\mathrm{ISRR} = \frac{\mathrm{IR}}{\mathrm{AU}} \times 100\%, \mathrm{ISCR} = \frac{\mathrm{IC}}{\mathrm{IR}} \times 100\% \tag{8}$$

where AU is the number of abnormal signals identified by the technician through voice listening and the waterfall graph of the digital sweep spectrum, AR is the number of abnormal signals correctly identified by the algorithm, AM is the number of normal signals incorrectly identified as abnormal signals by the algorithm, IR is the number of abnormal signals found by the interfering source, and IC is the number of interfering source signals correctly identified.

ASRR and ASMR can reflect the recognition effect of signal dwell time listening scheme on directly or indirectly generated abnormal signals. ISRR and ISCR reflect the recognition effect of the interference source identification method on the interference source of indirectly generated abnormal signals.

At P1 and P3. We did not detect an abnormal signal. At P2, we found a total of 18 abnormal signals. Upon listening to the voice content to verify the experimental results, only 2 of the signals were determined to be illegal broadcast generated intermodulation

signals, while the other abnormal signal band carried passive interference signals without carrying any information. At P4, we discovered 22 abnormal signals, and practically every abnormal signal could be obtained with at least one type of voice information through FM or AM demodulation.

At P2. The interference source identification method identified 3 sources of abnormal signals with 2 of them being correctly identified and one being incorrectly identified. At P4, the interference source of 5 abnormal signals is stably identified, among them, 4 interference sources are correct. As Fig. 8, we exemplify the illegal broadcast information obtained at the P4 in a certain period. The interference source identification algorithm continuously and stably monitored 117.45MHz as the intermodulation signal resulting from 98.675MHz and 101.25MHz. Upon verification through demodulation, we found that the talk show content on 98.675MHz and the marketing content of dietary supplements on 101.25MHz could be heard on 117.45MHz, where broadcasting on 101.25MHz is illegal.

The experimental results indicate that our scheme has better feasibility. For the 87MHz~137MHz frequency band, through the three steps of signal-to-noise separation, abnormal signal identification and interference source identification, it can effectively identify the abnormal radio interference in the approach control and tower control phases of civil aviation communication. It is beneficial for relevant law enforcement officers to control illegal FM broadcasting. In order to effectively ensure the safety of civil aviation passenger transportation, it is necessary to continuously monitor illegal stations. Our proposed method can be utilized to deploy multiple monitoring stations in the tower control and access control areas near airports for continuous monitoring and to cooperate with the relevant law enforcement agencies to manage the situation according to the law.

7 Conclusions

In this paper, we propose an abnormal signal monitoring and interference source identification method applied to the civil aviation communication security system. In order to realize the auxiliary monitoring of electromagnetic environment for civil aviation communication frequency band, we first obtain the signal frequency range of broadcasting frequency band and civil aviation communication frequency band through the adaptive signal-to-noise separation method, and then use the real-time abnormal signal monitoring method based on the signal residence time to obtain the abnormal signals in the civil aviation communication frequency band, and finally use the interference source identification method based on the Pearson's correlation coefficient to identify the interference

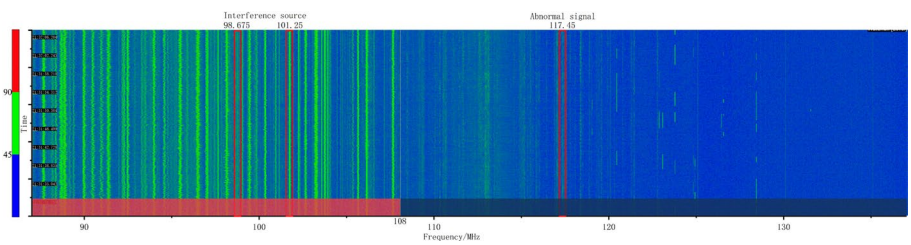

Fig. 8 Digital sweep frequency spectrum waterfall

source of the abnormal signals. We conducted several experiments near an airport to demonstrate that our method provides effective auxiliary monitoring. It helps technicians monitor interference sources in civil aviation communication in real-time, conveniently, quickly, and at a low cost. Additionally, during our practical application, we discovered many stations conducting illegal broadcasting, which seriously threatens civil aviation safety and should attract the attention of relevant departments.

Acknowledgements
Not applicable.

Author Contributions
Mingsheng Zhou completed the main innovative ideas and experiments of the article, Mingming Kong provided the experimental equipment and technical guidance for the work, Yuan Ye provided project fund support and data analysis, Binbin Deng assisted in the experiments and article writing, and Yulin Tang provided data support and data analysis. All authors read and approved the final manuscript.

Funding
This work was supported in part by the Key R&D Project implemented jointly by Sichuan and Chongqing in 2020 under Grant cstc2020jscx-cylhX0004; and the Natural Science Foundation of Ningxia Hui Autonomous Region in 2021 under grant No.2021AAC03439.

Availability of data and materials
No datasets were generated or analyzed during the current study.

Declarations

Competing interests
The authors declare no conflict of interest.

Received: 25 February 2024 Accepted: 16 September 2024
Published online: 27 September 2024

References

1. R. Johannessen, S. Gale, M. Asbury, Potential interference sources to gps and solutions appropriate for applications to civil aviation. In: Proceedings of the 45th annual meeting of the institute of navigation (1989), 195–201 (1989)
2. I. Fernández-Hernández, T. Walter, K. Alexander, B. Clark, E. Châtre, C. Hegarty, M. Appel, M. Meurer, Increasing international civil aviation resilience: A proposal for nomenclature, categorization and treatment of new interference threats. In: Proceedings of the 2019 international technical meeting of the institute of navigation, pp. 389–407 (2019)
3. M. De Angelis, R. Fantacci, S. Menci, C. Rinaldi, Analysis of air traffic control systems interference impact on galileo aeronautics receivers. In: IEEE international radar conference, 2005., pp. 585–595 (2005). IEEE
4. X. Zhang, Z. Luo, G. Kang, Analysis and research on the interference of civil aviation radio navigation equipment. In: Journal of Physics: Conference Series, 2209, 012011 (2022). IOP Publishing
5. B. Kamali, An overview of vhf civil radio network and the resolution of spectrum depletion. In: 2010 Integrated communications, navigation, and surveillance conference proceedings, pp. 4–1 (2010). IEEE
6. R. Zheng, X. Li, Y. Chen, An overview of cognitive radio technology and its applications in civil aviation. Sensors **23**(13), 6125 (2023)
7. K. Piamrat, A. Ksentini, J.-M. Bonnin, C. Viho, Radio resource management in emerging heterogeneous wireless networks. Comput. Commun. **34**(9), 1066–1076 (2011)
8. C. Zhou, S. He, J. Ye, P. Jia, Design and implementation of ground terminal for aerial radio monitoring system based on uav. In: Journal of Physics: Conference Series, 1626, 012084 (2020). IOP Publishing
9. G. Zhou, T. He, J.A. Stankovic, T. Abdelzaher, Rid: Radio interference detection in wireless sensor networks. In: Proceedings IEEE 24th annual joint conference of the IEEE computer and communications societies., 2, 891–901 (2005). IEEE
10. K.-S. Lee, A study on the aviation safety policy and enhancement of aviation safety for low cost carriers in Korea. Korean J. Air & Space Law and Policy **24**(2), 69–104 (2009)
11. A. Haniz, G.K. Tran, K. Sakaguchi, J.-i. Takada, T. Yamaguchi, T. Mitsui, S. Arata, Construction and interpolation of a multi-frequency radio map. In: 2019 International conference on robotics, electrical and signal processing techniques (ICREST), pp. 632–637 (2019). IEEE
12. S.H. Jung, B.-C. Moon, D. Han, Performance evaluation of radio map construction methods for wi-fi positioning systems. IEEE Trans. Intell. Transp. Syst. **18**(4), 880–889 (2016)
13. F. Zhou, C. Wang, G. Wu, Y. Wu, Q. Wu, N. Al-Dhahir, Accurate spectrum map construction for spectrum management through intelligent frequency-spatial reasoning. IEEE Trans. Commun. **71**, 3932 (2023)
14. X.-L. Huang, Y. Gao, X.-W. Tang, S.-B. Wang, Spectrum mapping in large-scale cognitive radio networks with historical spectrum decision results learning. IEEE Access **6**, 21350–21358 (2018)

15. T. Fujii, Smart spectrum management for v2x. In: 2018 IEEE international symposium on dynamic spectrum access networks (DySPAN), pp. 1–8 (2018). IEEE
16. Y.-Q. Xu, B. Zhang, G. Ding, B. Zhao, S. Li, D. Guo, Radio environment map construction based on spatial statistics and Bayesian hierarchical model. IEEE Trans. Cogn. Commun. Netw. **7**(3), 767–779 (2021)
17. V. Landon, A study of the characteristics of noise. Proceed. Inst. Radio Eng. **24**(11), 1514–1521 (1936)
18. G.C. Bjorklund, M. Levenson, W. Lenth, C. Ortiz, Frequency modulation (fm) spectroscopy: theory of lineshapes and signal-to-noise analysis. Appl. Phys. B **32**, 145–152 (1983)
19. H.T. Friis, Noise figures of radio receivers. Proc. IRE **32**(7), 419–422 (1944)
20. J. Ely, Electromagnetic interference to flight navigation and communication systems: new strategies in the age of wireless. In: AIAA guidance, navigation, and control conference and exhibit, p. 6361 (2005)
21. P. Kowalski, R. Smyk, Review and comparison of smoothing algorithms for one-dimensional data noise reduction. In: 2018 International interdisciplinary PhD workshop (IIPhDW), pp. 277–281 (2018). IEEE
22. M. Plass, M. Stone, Curve-fitting with piecewise parametric cubics. In: Proceedings of the 10th annual conference on computer graphics and interactive techniques, pp. 229–239 (1983)
23. R.M. Haralick, S.R. Sternberg, X. Zhuang, Image analysis using mathematical morphology. IEEE Trans. Pattern Anal. Mach. Intell. **4**, 532–550 (1987)
24. G. Tian, J. Zhou, X. Li, D. Li, Comprehensive experimental research on complex electromagnetic environment of aircraft. In: Journal of Physics: Conference Series, 1601, 022043 (2020). IOP Publishing
25. S.T. Acton, Fast algorithms for area morphology. Digit. Signal Process. **11**(3), 187–203 (2001)
26. R. Wu, Q. Shi, S. Wang, J. Ma, Adaptive interference suppression for civil aviation vhf air-to-ground communication based on constant modulus array. In: 2007 15th International conference on digital signal processing, pp. 67–70 (2007). IEEE
27. I. Cohen, Y. Huang, J. Chen, J. Benesty, J. Benesty, J. Chen, Y. Huang, I. Cohen, Pearson correlation coefficient. In: Noise Reduction in Speech Processing, (Springer, Heidelberg, 2009), 1–4
28. J. Pieper, *Standard Commands for Programmable Instruments* (SCPI Consortium ACEA, Wierden, The Neteherlands, 1998)
29. M. Zhou, Identification-of-interference-sources-dataset. Zenodo (CERN European Organization for Nuclear Research) (2023). https://doi.org/10.5281/zenodo.8022653

Publisher's Note